A Nonlinear, Robust Station–Season Index for Quantifying Fine–Coarse Mixture Regimes in Particulate Matter

D. Sierra-Porta[a], Isabella S. Arrieta-Guardo[a], Jose F. Gonzalez-Ortiz[a], and Eduardo A. Negrin-Perez[a]

[a]Escuela de Transformación Digital. Universidad Tecnológica de Bolívar. Parque Industrial y Tecnológico Carlos Vélez Pombo Km 1 Vía Turbaco. Cartagena de Indias, 130010, Bolívar, Colombia

May 11, 2026

Abstract

The objective of this study is to develop and evaluate an interpretable, robust station–season index that characterizes fine–coarse particulate-matter mixture regimes using routinely available regulatory monitoring data. Using EPA AQS daily $PM_{2.5}$ and PM_{10} observations (2022–2024), we computed the daily fine fraction $f(t) = PM_{2.5}(t)/PM_{10}(t)$ and coarse mass $PM_c(t) = \max\{PM_{10}(t) - PM_{2.5}(t), 0\}$. Each station–season–year was summarized by robust statistics: the median fine fraction f_{med}, median $PM_{2.5}$ $PM_{2.5,\text{med}}$, and a coarse-tail burstiness metric $B_c = \log(1 + PM_{c,\text{p90}}) - \log(1 + PM_{c,\text{med}})$. We then defined a nonlinear robust screening index,

$$S_{\text{NLR}} = \left[\log(1 + PM_{2.5,\text{med}})\right]^{\gamma} f_{\text{med}}^{\alpha} \exp(-\beta B_c),$$

with fixed parameters $\alpha = 0.55$, $\beta = 1.6$, and $\gamma = 1.2$, designed to increase with typical fine-dominant exposure and decrease with stronger coarse-tail influence. Analyses used $n = 240$ stations with consistent multi-year coverage, stratified by location setting (Suburban; Urban and center city) and land use (Residential; Commercial), with group differences summarized by median contrasts and nonparametric bootstrap confidence intervals. Seasonality dominates: S_{NLR} is lowest in spring (MAM) and highest in summer (JJA) across settings. Land-use contrasts are generally modest, although in DJF within Urban and center city, Residential stations show higher S_{NLR} than Commercial stations. Overall, S_{NLR} provides an interpretable, robustness-oriented tool for comparing fine–coarse mixture regimes using widely available monitoring data, rather than for source attribution or health-outcome inference.

Keywords: Particulate matter; $PM_{2.5}$; PM_{10}; $PM_{2.5}/PM_{10}$ ratio; fine fraction; composite index; coarse-tail burstiness; robust statistics; seasonality; air-quality monitoring; EPA AQS; land use; urbanicity

1 Introduction

Particulate matter (PM) remains one of the most consequential air pollutants for public health and environmental management. In the United States, regulatory monitoring networks operated under the U.S. Environmental Protection Agency (EPA) routinely report PM with aerodynamic diameters below 10 µm (PM_{10}) and 2.5 µm ($PM_{2.5}$), providing a long-running observational basis for spatially explicit assessment across heterogeneous environments. Recent regulatory actions further underscore the relevance of robust PM characterization at scale, including the strengthening of the primary annual $PM_{2.5}$ National Ambient Air Quality Standard (NAAQS) to 9.0 µg/m^3 [1, 2].

A central challenge is that PM is not a single entity but a mixture whose size partition reflects distinct sources and atmospheric processes. Fine particles ($PM_{2.5}$) are often dominated by combustion emissions and secondary formation, whereas coarse particles ($PM_{2.5-10}$) are more strongly linked to mechanical generation and resuspension, including wind-blown dust, road dust, construction, and other surface processes. Synoptic-scale episodes such as wildland-fire smoke, dust intrusions, and stagnation can transiently reshape this partition over broad regions, producing shifts that are not well represented by annual or seasonal means [3–11].

A growing literature shows that stratifying air-quality observations by land use and the urbanization gradient improves inference on dominant drivers and exposure disparities [12–17]. Urban cores and transportation corridors

tend to sustain elevated fine-particle burdens, while rural and agricultural regions can exhibit distinct seasonal behavior due to fertilizer and livestock-related precursors and regional transport [18, 19]. At the same time, compositional and seasonal contrasts between remote and urban settings indicate that both primary emissions and atmospheric chemistry vary strongly with season and region, motivating monitoring-derived descriptors that remain comparable under heterogeneous regimes [20].

A commonly used proxy for the fine–coarse partition is the ratio $PM_{2.5}/PM_{10}$ (or its complement), which is convenient and interpretable but can be fragile as a single-number summary [21, 22]. Ratio-only approaches are sensitive to shared-denominator effects and can yield misleading contrasts under measurement noise or when the numerator and denominator co-vary [23]. In regulatory monitoring, additional fragility arises from mass-measurement artifacts and quality-control issues that can distort tails and even produce implausible readings, especially when coarse fractions are inferred by subtraction rather than directly measured [24, 25]. In particular, two station–season distributions with similar medians can differ sharply in the frequency and amplitude of coarse-dominated excursions, which are often signatures of dust/resuspension regimes and carry distinct implications for screening and management [26]. These limitations motivate an index that is (i) robust to outliers and reporting artifacts, (ii) nonlinear in a way that respects bounded fractions, and (iii) sensitive to coarse episodic coarse influence without requiring chemically speciated measurements.

Here we introduce a *nonlinear, robust station–season index* to quantify fine–coarse mixture regimes using only routinely available $PM_{2.5}$ and PM_{10} data from EPA monitoring sites [27]. The index is constructed at the station–season (and year) level using robust distributional summaries that capture the typical fine fraction, the intensity of fine-particle exposure, and coarse episodic coarse influence (tail intensity and event frequency). To avoid pseudo-replication from serially correlated daily measurements, we treat station–season–year aggregates as the unit of inference and quantify uncertainty via resampling-based intervals and distributional contrasts.

The contribution of this study is not the general idea of a composite particulate-matter index, which is conceptually well established, but the development of a *robust, interpretable, and reproducible* station–season–year framework for fine–coarse mixture-regime characterization using routinely reported $PM_{2.5}/PM_{10}$ data. Specifically, we combine robust distributional summaries of fine-particle level and fine fraction with a coarse-tail penalty in a nonlinear score, and evaluate uncertainty and parameter robustness within a consistent network-wide analysis pipeline.

Specifically, we (i) define a bounded, nonlinear index that integrates robust summaries of fine fraction, fine-particle intensity, and coarse episodic coarse influence; (ii) provide stratified regime comparisons across land-use and location-setting classes; and (iii) assess seasonal contrasts with uncertainty estimates designed for heterogeneous station coverage.

Our scope is intentionally complementary to chemically speciated source apportionment. By relying on widely reported $PM_{2.5}$ and PM_{10}, the proposed index supports rapid, interpretable, and scalable screening across heterogeneous U.S. environments, helping identify where mixture regimes shift seasonally and where coarse-dominated episodic coarse influence may be most prominent. The remainder of this article describes the data sources and quality-control criteria, the index construction and robustness checks, and the resulting spatial and seasonal regime patterns by land use and location setting.

Accordingly, the aim of this work is not to propose a universally optimal PM mixture index, but to introduce and evaluate a practical screening metric (S_{NLR}) and accompanying analytical workflow for comparing station-scale fine–coarse regimes across seasons, land-use categories, and urbanicity strata under a robustness-oriented design.

2 Data and methods

2.1 Data

We used pre-generated daily summary files from the EPA AirData portal (AQS Data Mart extracts) for 2022–2024 (`https://www.epa.gov/aqs/obtaining-aqs-data`). Our core analysis relies on regulatory-grade particulate mass measurements: $PM_{2.5}$ Federal Reference Method / Federal Equivalent Method (FRM/FEM; parameter code 88101; `daily_88101_YYYY.zip`) and PM_{10} mass (81102; `daily_81102_YYYY.zip`) [28]. For optional quality-control and sensitivity checks (not used in the main index construction), we also retrieved $PM_{2.5}$ non-FRM/FEM "FRM-like" mass (88502; `daily_88502_YYYY.zip`) and coarse particulate matter $PM_{2.5-10}$ (86101; `daily_86101_YYYY.zip`) [28]. Files were obtained from the AirData pre-generated downloads page (`https://aqs.epa.gov/aqsweb/airdata/download_files.html`).

Each archive contains one record per monitor and local day, reporting a daily summary concentration (the *Arithmetic Mean* over valid sub-daily observations, as defined in AQS summary views) together with monitor identifiers and site descriptors (`https://www.epa.gov/sites/default/files/2017-03/documents/aqs_data_dictionary.`

pdf). We concatenated yearly archives (2022–2024) within each parameter, retained the minimal fields required for merging and stratification (Date Local, Arithmetic Mean, latitude/longitude, land-use class, and location setting), removed ancillary fields not used downstream (e.g., method text, addresses), and dropped occasional duplicate rows arising from file refreshes.

We harmonized land-use labels across years and retained the three location-setting categories used throughout (Urban and center city, Suburban, Rural). Parameter-specific tables were then merged at the monitor–day level using the AQS site identifier (State Code, County Code, Site Num) and the Parameter Occurrence Code (POC) [29], together with Date Local, so that $PM_{2.5}$ and PM_{10} refer to collocated instruments on the same local day. In the analyses that follow, $PM_{2.5}$ FRM/FEM (88101) and PM_{10} (81102) form the primary data stream for constructing the station–season index; 88502 and 86101 are reserved for robustness and consistency checks only.

2.2 Network composition and completeness

The analytical monitoring network spans a broad urbanization gradient and multiple land-use contexts. After applying the completeness and merge requirements described above, the final sample comprises **240** EPA monitors with sufficient daily coverage during 2022–2024 [30]. This retained network reflects both the spatial distribution of regulatory monitoring and the additional requirement of same-day availability of $PM_{2.5}$ and PM_{10} for mixture-based metrics. As a result, the analytical sample should be interpreted as a high-completeness subset of the broader AQS inventory rather than a nationally representative random sample.

The retained network includes $n = 240$ monitors spanning all three location-setting classes (Rural $n = 44$, Suburban $n = 103$, Urban and center city $n = 93$) and five land-use groupings (Residential $n = 118$, Commercial $n = 70$, Agricultural $n = 20$, Industrial $n = 16$, Other/Minor $n = 16$). Table 1 reports the joint distribution across land use and location setting.

Table 1: Cross-classification of retained stations by land use and location setting ($n = 240$). Column and row totals provide the marginal counts.

Land use	**Rural**	**Suburban**	**Urban and center city**	**Total**
Agricultural	20	0	0	20
Commercial	4	24	42	70
Industrial	3	7	6	16
Other/Minor	8	4	4	16
Residential	9	68	41	118
Total	**44**	**103**	**93**	**240**

Because some strata are inherently sparse (e.g., industrial sites within specific settings, or the heterogeneous Other/Minor category), downstream analyses emphasize robust summaries and uncertainty intervals at the station–season (and year) level. In particular, we interpret small-count strata cautiously and focus inferential contrasts on comparisons with adequate station coverage (e.g., Residential vs. Commercial within Suburban and Urban and center city settings). Figure 1 shows the geospatial distribution of retained stations and confirms that the network provides coverage across major U.S. regions, with denser sampling in coastal and urban corridors and sparser coverage in parts of the interior West.

2.3 Methods

We defined climatological seasons by calendar months: Winter (December–February; DJF), Spring (March–May; MAM), Summer (June–August; JJA), and Autumn (September–November; SON). Each daily record inherits the season label from its local date. To respect temporal dependence and episodic structure in daily air-quality time series, we treat the *station–season–year* as the unit of analysis [31, 32]. For each monitor and season we compute year-specific robust summaries (2022–2024) from daily $PM_{2.5}$ and PM_{10}; comparisons across strata are performed on these seasonal aggregates rather than on daily observations.

For each monitor-day with valid $PM_{2.5}$ and PM_{10}, we computed the fine fraction [33, 34]

$$f(t) = \frac{\mathrm{PM}_{2.5}(t)}{\mathrm{PM}_{10}(t)}\,, \tag{1}$$

and the coarse mass by difference,

$$\mathrm{PM}_c(t) = \max\{\mathrm{PM}_{10}(t) - \mathrm{PM}_{2.5}(t),\, 0\}. \tag{2}$$

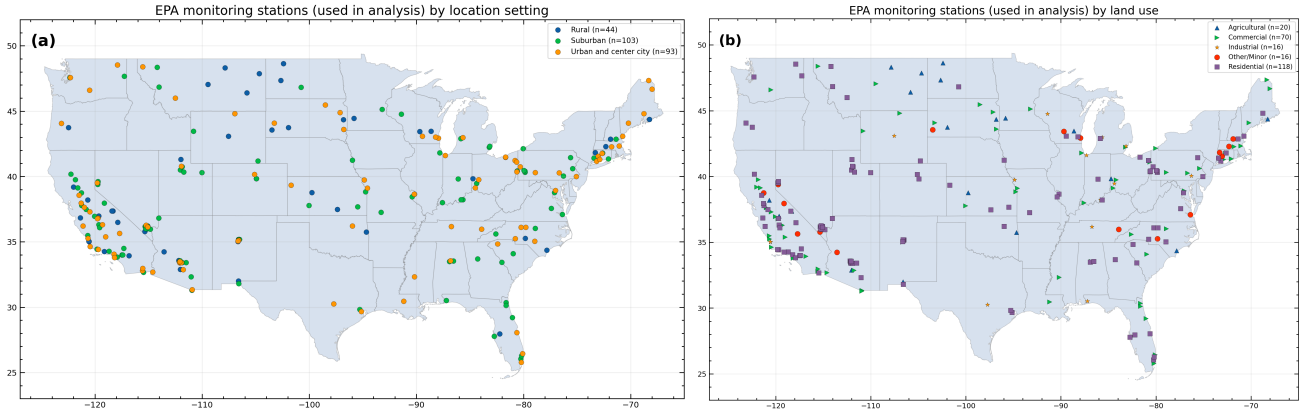

Figure 1: Geospatial distribution of EPA monitoring stations retained for analysis ($n = 240$) after completeness screening (2022–2024). Panel (a) shows the urbanization gradient (Rural/Suburban/Urban and center city); panel (b) shows the land-use grouping used for stratified analyses (land use).

Days lacking either $PM_{2.5}$ or PM_{10} were excluded from mixture calculations. Ratios were computed only when denominators were strictly positive; non-finite results were treated as missing. Fine fractions were computed only when $PM_{10}(t) > 0$; non-finite results were treated as missing.

Quality control proceeded in three layers. First, we enforced numerical validity at the daily level by removing records with missing values, non-positive denominators, or non-finite derived quantities. Second, to avoid mixing non-collocated instruments, $PM_{2.5}$ and PM_{10} were matched at the monitor–day level using the AQS site identifier (State Code, County Code, Site Num) together with the Parameter Occurrence Code (POC) and Date Local, ensuring that daily mixtures reflect the same physical site and instrument stream. Third, we applied a completeness screen at the station–parameter level over 2022–2024, retaining monitors with at least 1000 valid daily means in the primary regulatory series. For mixture-based calculations, only days with same-day availability of both $PM_{2.5}$ and PM_{10} contribute to station–season summaries; all other days are ignored for mixture metrics.

Within each station–season–year group, we summarized (i) the typical fine fraction by the median f_{med}, (ii) the typical fine-particle level by the median $PM_{2.5,\mathrm{med}}$, and (iii) coarse episodic coarse influence via a tail-intensity burst metric based on the 90th percentile and median of $PM_c(t)$,

$$B_c = \log\bigl(1 + \mathrm{PM}_{c,\mathrm{p90}}\bigr) - \log\bigl(1 + \mathrm{PM}_{c,\mathrm{med}}\bigr), \tag{3}$$

where $PM_{c,\mathrm{p90}}$ and $PM_{c,\mathrm{med}}$ are computed within the station–season–year group. The log transform reduces sensitivity to extreme values while preserving monotonicity. This quantity summarizes *coarse-tail burstiness* as a robust tail-to-center contrast on a log scale, reducing sensitivity to extremes while preserving monotonicity.

Here, B_c is interpreted as a *distributional coarse-tail intensity* descriptor (upper-tail contrast relative to the median), not as a direct measure of temporal clustering, intermittency, or event frequency.

We define the nonlinear robust index S_{NLR} as

$$S_{\mathrm{NLR}} = \Bigl[\log\bigl(1 + \mathrm{PM}_{2.5,\mathrm{med}}\bigr)\Bigr]^{\gamma} \Bigl[f_{\mathrm{med}}\Bigr]^{\alpha} \exp\bigl(-\beta\, B_c\bigr), \tag{4}$$

with fixed parameters $\alpha = 0.55$, $\beta = 1.6$, and $\gamma = 1.2$.

We set $(\alpha, \beta, \gamma) = (0.55, 1.6, 1.2)$ to balance the typical dynamic ranges of the three ingredients in Eq. (4), so that no single component (e.g., the burstiness penalty) dominates the score across the observed station–season distributions. The main qualitative findings (MAM minima, JJA maxima, and the DJF urban Residential>Commercial contrast) remain unchanged under reasonable one-at-a-time perturbations of (α, β, γ) (e.g., $\pm 20\%$).

The S_{NLR} was designed as an *interpretable descriptive index* for station-scale mixture-regime screening rather than as a predictive model or an outcome-optimized estimator. Accordingly, the functional form was selected using design principles of monotonicity, scale balance, and interpretability, rather than formal predictive optimization or model selection. The multiplicative structure was used to represent a conjunctive regime score, so that high S_{NLR} values arise when fine-particle loading and fine fraction are jointly elevated while coarse-tail burstiness remains limited. The logarithmic transformation was applied to $PM_{2.5,\mathrm{med}}$ to reduce scale dominance and compress right-skewed variation, whereas the fine-fraction term is already dimensionless and bounded; the exponential term was used as a smooth monotonic penalty for coarse-tail burstiness, with tunable sensitivity. The qualitative roles and signs of α, β,

and γ were conceptually motivated by the intended behavior of the index, whereas the specific baseline values were selected through simple empirical balancing of component dynamic ranges and practical interpretability (i.e., to avoid dominance of a single component), rather than through outcome-based tuning. To assess dependence on this baseline parameterization, we performed a quantitative sensitivity analysis over ±20% perturbations (full grid and one-at-a-time variations), reported in Section 3.1.

We do not claim this parameterization to be uniquely optimal, but rather a transparent, robustness-checked baseline design for comparative regime characterization.

The index increases with higher typical fine fraction and higher typical $PM_{2.5}$ intensity, and it is penalized exponentially by coarse-tail burstiness. In implementation, we clip $f_{\text{med}} \in [0, 1]$ and enforce non-negativity for $PM_{2.5,\text{med}}$ and PM_c summaries to avoid spurious values from rare reporting artifacts [35–37].

Stations were stratified by land use and location setting, and results are reported seasonally. For focused contrasts, we compared Residential versus Commercial regimes within each season and location setting using station–season–year values of S_{NLR}. Differences were summarized by the difference in medians,

$$\Delta_{\text{med}} = \text{median}(S_{\text{NLR}}^{\text{Res}}) - \text{median}(S_{\text{NLR}}^{\text{Com}}),$$

and uncertainty was quantified via nonparametric bootstrap within each (season, location setting) stratum. Specifically, within a given stratum we resampled with replacement the Residential and Commercial S_{NLR} values independently, preserving the original sample sizes, and recomputed Δ_{med} over $B = 4000$ bootstrap replicates to form a two-sided 95% percentile interval [38]. Strata with fewer than 20 station–season–year units in either group were omitted to avoid unstable rank-based summaries. This procedure yields uncertainty for between-group regime differences while avoiding pseudo-replication from serially correlated daily measurements.

The station–season–year aggregation was adopted to reduce temporal dependence among daily observations and to avoid pseudo-replication in cross-station comparisons. This choice, however, also defines the interpretative scope of the S_{NLR}: seasonal aggregation may attenuate short-lived event-scale contrasts (e.g., dust outbreaks or wildfire episodes) by averaging transient signals into broader seasonal summaries. Alternative windows (e.g., monthly, rolling, or event-centered aggregation) could increase sensitivity to episodic contrasts, but would likely involve trade-offs in robustness, effective sample size, and sensitivity to missingness and short-term variability. Accordingly, the S_{NLR} is interpreted here as a seasonal station-level screening/diagnostic index rather than an event-detection metric.

All analyses were performed in Python using `pandas`, `numpy`, and `scipy` for data processing and inference, and `matplotlib` for visualization. The full pipeline reproduces screening criteria, derived-variable construction, and resampling-based uncertainty estimates using publicly available EPA AirData daily files for 2022–2024 (`https://aqs.epa.gov/aqsweb/airdata/download_files.html`) [39, 40].

3 Results and Discussion

3.1 Parameter-sensitivity analysis of the S_{NLR}

To assess whether the main findings depend on a narrow choice of S_{NLR} parameters, we performed a quantitative sensitivity analysis around the baseline parameterization $(\alpha, \beta, \gamma) = (0.55, 1.6, 1.2)$. We evaluated a ±20% perturbation range for each parameter using (i) a full $3 \times 3 \times 3$ grid (27 configurations) and (ii) one-at-a-time variations while holding the remaining parameters fixed at baseline. For each alternative parameter set, S_{NLR} was recomputed on the same station–season–year aggregates, and stability was evaluated on the main analytical subset (Residential/Commercial × Suburban/Urban and center city).

For the full $3 \times 3 \times 3$ sensitivity grid, each parameter was evaluated at its baseline value and at ±20%: $\alpha \in \{0.44, 0.55, 0.66\}$, $\beta \in \{1.28, 1.60, 1.92\}$, and $\gamma \in \{0.96, 1.20, 1.44\}$. All 27 combinations were recomputed on the same station–season–year aggregates (including the baseline configuration), and one-at-a-time (OAT) analyses varied one parameter across the same three-point set while holding the remaining two fixed at baseline.

Across the full 27-configuration grid, rank agreement with the baseline S_{NLR} remained very high (Spearman correlation vs. baseline: median = 0.994, minimum = 0.981). Stability was also strong at the tails of the distribution: top-decile overlap with the baseline ranking had median = 0.936 (minimum = 0.873), and bottom-decile overlap had median = 0.936 (minimum = 0.855). In addition, the principal qualitative conclusions were preserved in all tested configurations: the global seasonal ordering remained unchanged (MAM as the lowest-median season and JJA as the highest-median season), and the key Urban-DJF contrast (Residential median S_{NLR} > Commercial median S_{NLR}) was retained in 100% of cases.

The one-at-a-time analysis yielded consistent conclusions. Relative to the baseline S_{NLR}, all one-parameter perturbations produced high rank concordance (Spearman $\rho = 0.994$–0.998), while the Urban-DJF Residential-

minus-Commercial median contrast remained positive throughout ($\Delta S_{\mathrm{NLR}} = 0.079$ to 0.114; baseline = 0.101). These results indicate that the selected parameterization affects the scale of the index and the magnitude of some contrasts, but does not alter the main qualitative structure of the results.

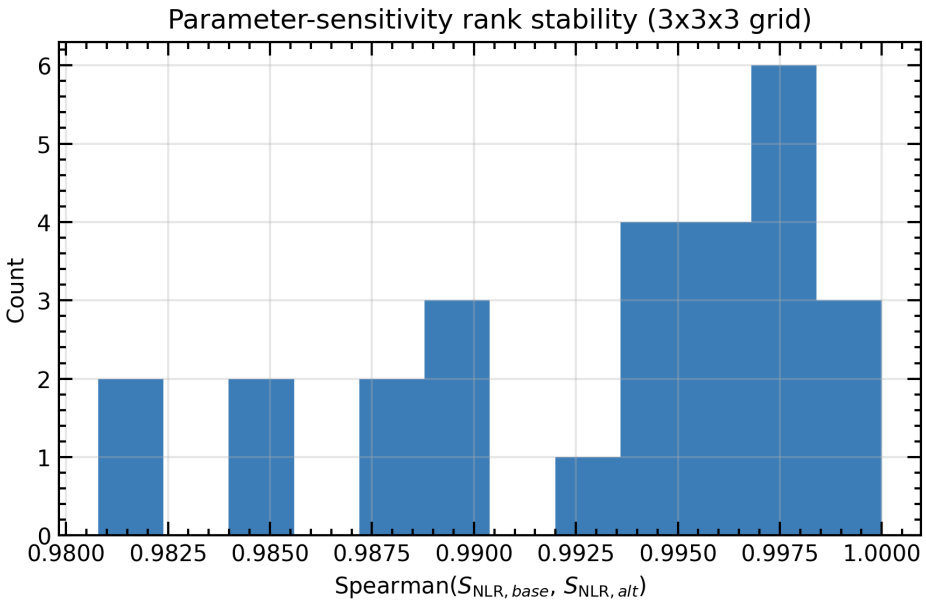

Figure 2: Parameter-sensitivity analysis of the S_{NLR} under ±20% perturbations of α, β, and γ around the baseline parameterization (0.55,1.6,1.2). The histogram summarizes rank agreement (Spearman correlation) between the baseline S_{NLR} and S_{NLR} values recomputed for all $3 \times 3 \times 3$ parameter combinations (27 configurations) on the main analytical subset. The distribution is concentrated near 1, indicating high rank stability across plausible parameter choices and supporting the robustness of the main qualitative conclusions to parameter variation.

Given this robustness, we retained the baseline parameter set $(\alpha, \beta, \gamma) = (0.55, 1.6, 1.2)$ for all primary analyses reported below. Figure 2 provides a compact visual summary of rank stability across the full parameter grid, while Table 2 reports the corresponding quantitative stability diagnostics.

3.2 Benchmarking S_{NLR} against simpler metrics and component-level summaries

To assess whether S_{NLR} provides information beyond simpler alternatives, we benchmarked it against (i) the median fine fraction $f_{\mathrm{med}} = \mathrm{median}(\mathrm{PM}_{2.5}/\mathrm{PM}_{10})$ (a conventional ratio-based summary), (ii) $\mathrm{PM}_{2.5,\mathrm{med}}$, (iii) the coarse-tail metric B_c, and (iv) a reduced composite without the coarse-tail penalty term. We evaluated both correlation structure (Pearson and Spearman) and stratified Residential–Commercial contrasts across the same season × setting strata used in the main analysis.

Correlation analyses indicate that S_{NLR} is related to, but not redundant with, any single component. In the main analytical subset, Spearman correlations between S_{NLR} and f_{med}, $\mathrm{PM}_{2.5,\mathrm{med}}$, and B_c were 0.567, 0.583, and -0.691, respectively (Pearson: 0.551, 0.530, and -0.661). These moderate correlations contrast with the relatively weak dependence among the components themselves (e.g., Spearman f_{med} vs $\mathrm{PM}_{2.5,\mathrm{med}} = 0.330$, f_{med} vs $B_c = 0.017$, $\mathrm{PM}_{2.5,\mathrm{med}}$ vs $B_c = -0.084$), consistent with the interpretation that the index combines partially distinct dimensions of mixture-regime behavior rather than simply re-scaling one variable.

The stratified benchmarking also helps define the practical scope of the index. Across all eight season × setting strata, S_{NLR} did not uniformly maximize Residential–Commercial separation relative to all simpler metrics, which we now state explicitly. However, in the key Urban-DJF stratum emphasized in the main results, S_{NLR} showed a stronger standardized median contrast (0.301, IQR-standardized) than f_{med} alone (0.043) and $\mathrm{PM}_{2.5,\mathrm{med}}$ alone (0.255), and was comparable to the reduced composite without the coarse-tail penalty (0.300). This supports the value of the composite formulation for the principal regime contrast highlighted in this study while avoiding the over-claim that it is universally superior in all strata.

Taken together, these results indicate that the main contribution of S_{NLR} is not universal discrimination gain over every simpler metric, but a compact and interpretable regime-oriented summary that jointly encodes fine loading, fine fraction, and coarse-tail influence in a robustness-checked framework.

Table 2: Compact summary of S_{NLR} parameter-sensitivity results under ±20% perturbations of α, β, and γ around the baseline parameterization $(0.55, 1.6, 1.2)$. Grid analysis includes all $3 \times 3 \times 3$ combinations (27 configurations). OAT = one-at-a-time perturbations (one parameter varied while the other two are fixed at baseline). Stability metrics are computed on the main analytical subset.

Metric	**Grid (27)**	**OAT**
Spearman correlation vs. baseline S_{NLR} (median)	0.994	–
Spearman correlation vs. baseline S_{NLR} (minimum)	0.981	0.994
Spearman correlation vs. baseline S_{NLR} (maximum)	–	0.998
Top-decile overlap with baseline ranking (median)	0.936	–
Top-decile overlap with baseline ranking (minimum)	0.873	–
Bottom-decile overlap with baseline ranking (median)	0.936	–
Bottom-decile overlap with baseline ranking (minimum)	0.855	–
Share preserving MAM as global seasonal minimum	1.00	1.00
Share preserving JJA as global seasonal maximum	1.00	1.00
Share preserving Urban-DJF Residential > Commercial	1.00	1.00
Urban-DJF (Residential–Commercial) median S_{NLR} contrast	–	0.079–0.114
Urban-DJF (Residential–Commercial) baseline contrast	0.101	

Table 3 benchmarks the baseline S_{NLR} against simpler and component-level alternatives. The correlation structure shows that S_{NLR} is related to, but not redundant with, any single component (e.g., Spearman $\rho = 0.567$ with f_{med}, $\rho = 0.583$ with $\mathrm{PM}_{2.5,\mathrm{med}}$, and $\rho = -0.691$ with B_c). In the key Urban-DJF stratum, S_{NLR} shows a stronger IQR-standardized Residential–Commercial contrast than the ratio-only metric (0.301 vs 0.043) and $\mathrm{PM}_{2.5,\mathrm{med}}$ alone (0.301 vs 0.255), while remaining comparable to the reduced composite without the coarse-tail penalty (0.300).

Table 3: Benchmarking of the baseline nonlinear regime index S_{NLR} against simpler and component-level metrics on the main analytical subset. Panel A reports Pearson and Spearman correlations with selected alternatives. Panel B reports Residential–Commercial contrasts in the key Urban-DJF stratum, including raw median differences, IQR-standardized median differences, and common-language effect size (CLE; probability that a randomly selected Residential unit exceeds a randomly selected Commercial unit).

Panel A. Correlation of S_{NLR} with simpler/component-level metrics		
Metric	**Pearson r**	**Spearman ρ**
f_{med} (median $\mathrm{PM}_{2.5}/\mathrm{PM}_{10}$ ratio)	0.551	0.567
$\mathrm{PM}_{2.5,\mathrm{med}}$	0.530	0.583
B_c (coarse-tail burstiness)	-0.661	-0.691
Reduced composite (no coarse-tail penalty)	0.685	0.703

Panel B. Key stratum benchmark: Urban and center city (DJF), Residential–Commercial			
Metric	**Median diff. (Res–Com)**	**IQR-std. diff.**	**CLE (Res>Com)**
S_{NLR} (baseline)	0.101	0.301	0.622
Reduced composite (no coarse-tail penalty)	0.174	0.300	0.614
f_{med}	0.011	0.043	0.583
$\mathrm{PM}_{2.5,\mathrm{med}}$	0.942	0.255	0.613
B_c	-0.050	-0.181	0.445

3.3 Baseline characterization of $\mathrm{PM}_{2.5}$, PM_{10}, and coarse-tail burstiness (B_c)

We begin by characterizing the seasonal distribution of $\mathrm{PM}_{2.5}$ and PM_{10} at the same unit of analysis used throughout (station–season–year), so that subsequent interpretation of the nonlinear regime index S_{NLR} is anchored in observable concentration patterns. Figure 3 summarizes the distributions of station-level seasonal medians for $\mathrm{PM}_{2.5,\mathrm{med}}$ and $\mathrm{PM}_{10,\mathrm{med}}$ by season, location setting, and land-use class.

Table 4 complements this visualization by reporting robust group medians with 95% bootstrap confidence intervals (CIs) for $\mathrm{PM}_{2.5,\mathrm{med}}$, $\mathrm{PM}_{10,\mathrm{med}}$, and a coarse-tail burstiness metric (denoted B_c).

Across strata, $\mathrm{PM}_{2.5,\mathrm{med}}$ exhibits comparatively compact seasonal distributions centered around ∼5–8 $\mu\mathrm{g/m}^3$, with moderate seasonal shifts and substantial within-stratum variability (Fig. 3). Differences between Residential

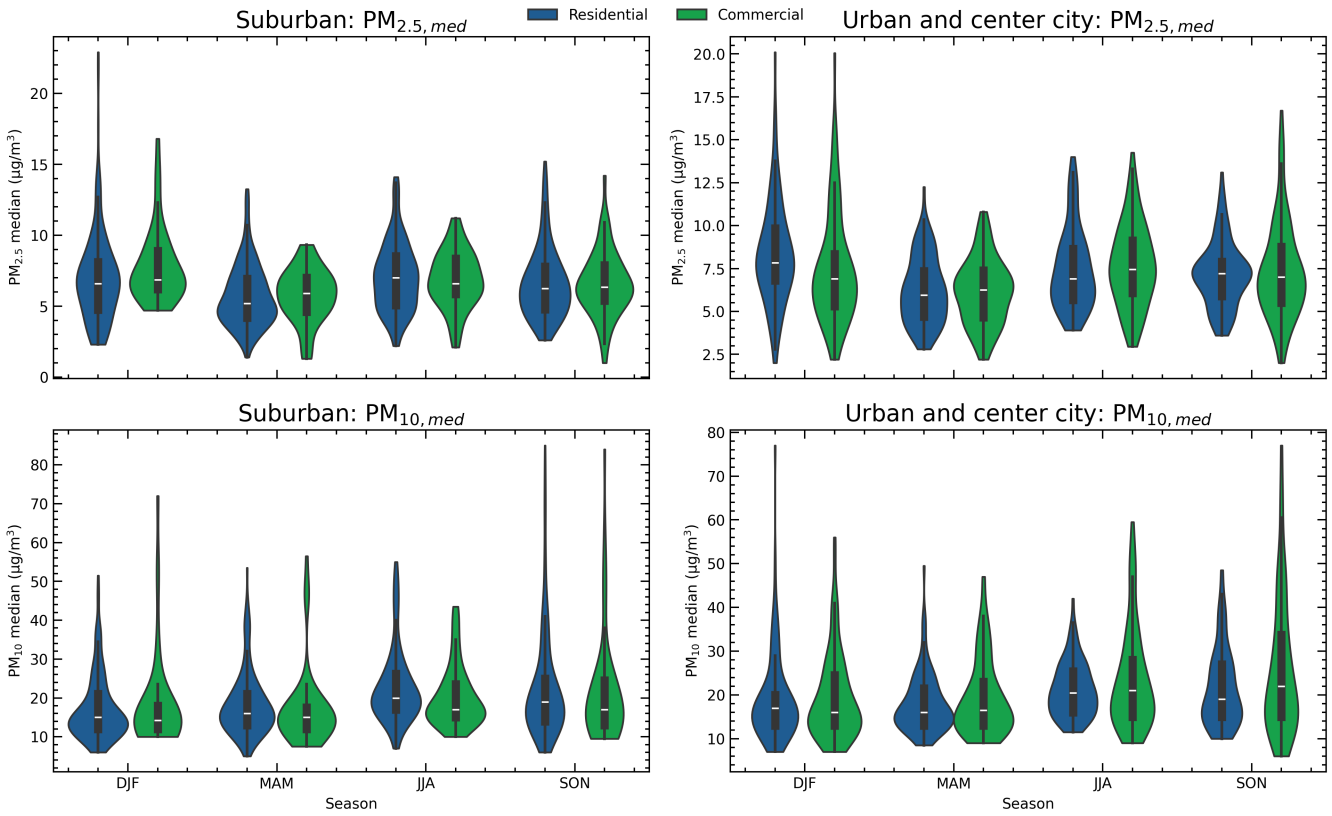

Figure 3: Seasonal distributions of station–season–year medians for $PM_{2.5}$ (top) and PM_{10} (bottom), stratified by location setting (columns) and land-use class (color).

and Commercial medians are typically modest relative to within-group spread, but some setting–season combinations show clearer separation. Notably, in Urban and center city during DJF, $PM_{2.5,\mathrm{med}}$ is higher in Residential (median 7.84 $\mu g/m^3$) than Commercial (6.90 $\mu g/m^3$), consistent with the upward shift visible in the winter violins (Table 4).

$PM_{10,\mathrm{med}}$ displays broader tails and more pronounced heterogeneity than $PM_{2.5,\mathrm{med}}$ across nearly all seasons and settings (Fig. 3), emphasizing the role of coarse contributions in shaping variability at seasonal scales. Seasonal contrasts in $PM_{10,\mathrm{med}}$ are particularly visible in warm and transition seasons for several strata. For example, in Suburban JJA, Residential shows higher $PM_{10,\mathrm{med}}$ (20.0 $\mu g/m^3$) than Commercial (17.0 $\mu g/m^3$), while $PM_{2.5,\mathrm{med}}$ differs only slightly (7.0 vs 6.6 $\mu g/m^3$; Table 4). This pattern illustrates that similar fine-mode central tendencies can occur under distinct total-mass (PM_{10}) environments, which is consequential when interpreting mixture-regime behavior.

Finally, coarse-tail burstiness, summarized by B_c, varies meaningfully across season, setting, and land use (Table 4). In Suburban DJF, B_c medians are comparable across land uses (0.663 in Commercial vs 0.644 in Residential), whereas in Urban and center city DJF the Residential group shows lower B_c (0.613) than Commercial (0.663). Importantly, B_c is a *distributional* descriptor based on the contrast between an upper quantile and the median of inferred coarse mass, so it reflects coarse-tail intensity relative to typical conditions rather than temporal clustering or event frequency per se. In this sense, B_c captures the tendency for coarse contributions to appear as stronger upper-tail excursions within the station–season distribution.

Taken together, the baselines in $PM_{2.5,\mathrm{med}}$, $PM_{10,\mathrm{med}}$, and coarse-tail burstiness (B_c) establish the empirical backdrop for the compound nonlinear regime index S_{NLR} analyzed next. In particular, Urban DJF combines higher typical fine mass (Residential > Commercial) with reduced B_c in Residential, a pattern revisited in the S_{NLR} decomposition below.

3.4 Land-use effects on the nonlinear regime index S_{NLR} across seasons

We now summarize the seasonal behavior of the nonlinear regime index S_{NLR} across land-use categories (Residential

Table 4: Baseline station–season–year characterization by season, location setting, and land-use class. Values are medians with 95% bootstrap confidence intervals; n counts station–season–year units.

setting	**season**	**land use**	**n**	B_c	$\mathbf{PM}_{10,\mathrm{med}}$	$\mathbf{PM}_{2.5,\mathrm{med}}$
Suburban	DJF	Commercial	44	0.663 [0.54, 0.775]	14.25 [13.0, 16.0]	6.85 [6.5, 7.8]
Suburban	DJF	Residential	159	0.644 [0.602, 0.674]	15.0 [14.0, 15.0]	6.6 [6.2, 7.12]
Suburban	JJA	Commercial	57	0.448 [0.426, 0.504]	17.0 [16.0, 20.5]	6.6 [6.15, 7.55]
Suburban	JJA	Residential	175	0.454 [0.42, 0.476]	20.0 [19.5, 21.0]	7.0 [6.35, 7.45]
Suburban	MAM	Commercial	53	0.558 [0.451, 0.727]	15.0 [13.5, 16.0]	5.9 [5.15, 6.65]
Suburban	MAM	Residential	175	0.594 [0.554, 0.627]	16.0 [15.5, 17.0]	5.2 [4.9, 5.7]
Suburban	SON	Commercial	59	0.598 [0.497, 0.632]	17.0 [15.0, 20.0]	6.35 [5.8, 6.8]
Suburban	SON	Residential	182	0.561 [0.537, 0.589]	19.0 [17.0, 20.0]	6.25 [5.9, 6.62]
Urban and center city	DJF	Commercial	93	0.663 [0.621, 0.725]	16.0 [14.5, 19.0]	6.9 [6.15, 7.35]
Urban and center city	DJF	Residential	100	0.613 [0.582, 0.677]	17.0 [15.0, 18.0]	7.84 [7.4, 8.64]
Urban and center city	JJA	Commercial	106	0.513 [0.448, 0.569]	21.0 [17.0, 23.0]	7.45 [7.05, 8.15]
Urban and center city	JJA	Residential	106	0.442 [0.406, 0.474]	20.5 [19.0, 22.0]	6.9 [6.5, 7.64]
Urban and center city	MAM	Commercial	106	0.608 [0.567, 0.665]	16.5 [15.0, 18.0]	6.25 [5.75, 6.65]
Urban and center city	MAM	Residential	105	0.627 [0.565, 0.65]	16.0 [15.0, 17.5]	5.95 [5.6, 6.45]
Urban and center city	SON	Commercial	110	0.579 [0.55, 0.631]	22.0 [18.0, 25.0]	7.0 [6.3, 7.35]
Urban and center city	SON	Residential	107	0.568 [0.515, 0.609]	19.0 [17.0, 22.0]	7.2 [6.8, 7.45]

Table 5: Seasonal summaries of S_{NLR} by season, location setting, and land-use category. Medians are shown with 95% bootstrap confidence intervals; n counts station–year–season units in each group.

Location setting	**Season**	n_{Res}	**Residential: median [95% CI]**	n_{Com}	**Commercial: median [95% CI]**
Suburban	DJF	159	0.511 [0.456, 0.559]	44	0.607 [0.505, 0.702]
Suburban	MAM	175	0.433 [0.386, 0.492]	53	0.469 [0.387, 0.567]
Suburban	JJA	175	0.584 [0.516, 0.657]	57	0.604 [0.515, 0.757]
Suburban	SON	182	0.466 [0.425, 0.502]	59	0.450 [0.392, 0.614]
Urban and center city	DJF	100	0.592 [0.541, 0.676]	93	0.491 [0.407, 0.559]
Urban and center city	MAM	105	0.465 [0.409, 0.509]	106	0.459 [0.390, 0.502]
Urban and center city	JJA	106	0.638 [0.586, 0.732]	106	0.600 [0.514, 0.699]
Urban and center city	SON	107	0.533 [0.501, 0.553]	110	0.492 [0.463, 0.548]

vs Commercial) and location settings (Suburban vs Urban and center city), using the same station–year–season units described above. Tables 5 and 6 report group medians and Residential–Commercial median differences with 95% bootstrap confidence intervals, while Figs. 4–6 and the DJF decomposition in Fig. 5 provide complementary distributional and component-level context.

A first-order feature of the data is the strong seasonal structure of S_{NLR} across both location settings (Table 5, Fig. 4). Medians are lowest in MAM and highest in JJA in all strata, indicating that the mixture regime shifts systematically across the annual cycle. Because S_{NLR} increases with typical $\mathrm{PM}_{2.5}$ and the typical fine fraction while penalizing coarse-tail burstiness, elevated JJA values are consistent with conditions that favor sustained fine-mode aerosol and/or a weaker influence of episodic coarse variability at the seasonal-median scale. Conversely, the MAM depression of S_{NLR} suggests either weaker persistence of fine-dominated conditions, stronger coarse-tail burstiness, or a mixture that includes more variable coarse contributions at the station–season scale.

The Residential–Commercial contrasts are comparatively subtle once uncertainty is accounted for (Table 6). Most seasonal differences are not distinguishable from zero at the 95% level given the observed within-group dispersion, indicating that land-use category by itself is not a strong separator of S_{NLR} at the median scale for most settings and seasons. The clearest exception is Urban and center city in DJF, where Residential exceeds Commercial (median difference 0.101 with a positive 95% CI). This DJF-specific separation is therefore the most robust land-use signal supported by the current analysis. This interpretation is also consistent with the broad overlap visible in the seasonal violin distributions (Fig. 4), where within-group dispersion often exceeds between-group shifts.

Several factors naturally limit land-use separability and help explain why most contrasts are weak. First, the land-use labels are coarse proxies for local source mixtures and may not capture key micro-environmental determinants such as near-road proximity, street canyons, industrial corridors, rail yards, construction intensity, or local dust/sea-salt influence [41, 42]. Second, the station network is not balanced across strata (e.g., Residential typically has larger n than Commercial in Suburban), which widens uncertainty for smaller groups and reduces

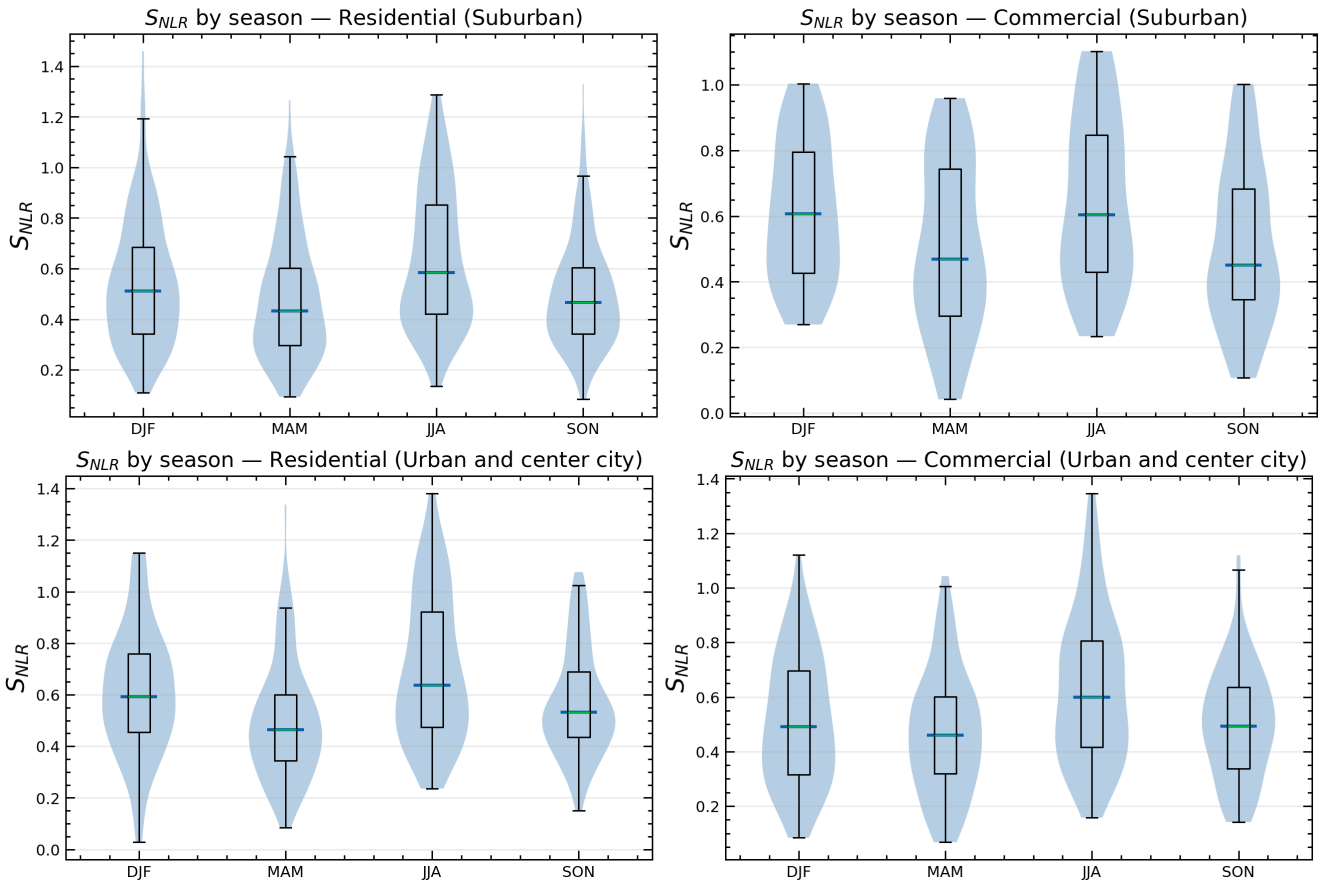

Figure 4: Seasonal distributions of S_{NLR} by land use. The violins emphasize seasonal shifts and within-group dispersion, showing MAM minima and JJA maxima across settings.

power to resolve modest shifts [43]. Third, meteorology can synchronize exposures across land-use types within a region (e.g., synoptic stagnation, frontal passages, or widespread resuspension episodes), increasing overlap between categories even when local sources differ [44, 45].

The distributional decomposition in DJF (Fig. 5) provides a mechanistic interpretation for the Urban DJF signal. In Urban and center city, higher S_{NLR} in Residential aligns with a combination of higher typical $\mathrm{PM}_{2.5}$ and fine fraction, together with modestly reduced coarse-tail burstiness, yielding a more stable fine-dominated exposure regime in winter. From an environmental perspective, winter conditions often feature shallower planetary boundary layers and more frequent stable stratification (including thermal inversions), which can reduce ventilation and favor pollutant accumulation near the surface. Such meteorological modulation is consistent with long-term observational evidence that boundary-layer height and inversion frequency exhibit a seasonal cycle and can be statistically linked to $\mathrm{PM}_{2.5}$ variability in urban environments [46–48]. Accordingly, the DJF Residential>Commercial separation in Urban sites should be interpreted as consistent with (rather than caused by) wintertime dispersion constraints operating on top of local emissions and site micro-environmental factors [46].

In this context, relatively small shifts in typical $\mathrm{PM}_{2.5}$ and mixture fraction can translate into a clearer separation in S_{NLR} than in seasons characterized by stronger vertical mixing. Consistent with this interpretation, the baseline summaries already show that Urban DJF Residential has higher $\mathrm{PM}_{2.5,\mathrm{med}}$ (7.84 vs 6.90 $\mu\mathrm{g/m}^3$) and lower B_c (0.613 vs 0.663) than Urban DJF Commercial (Table 4), while Fig. 5 indicates that wintertime differences in f_{med} can further reinforce the separation in S_{NLR}.

In Suburban DJF, the direction reverses (Commercial > Residential in the median), although the CI overlaps zero (Table 6). The DJF decomposition suggests that this is not driven by large $\mathrm{PM}_{2.5}$ differences but is compatible with subtle mixture differences: slightly higher fine fraction and comparable coarse-tail burstiness in Commercial relative to Residential. A plausible interpretation is that suburban Commercial sites may capture relatively steady fine-mode contributions associated with traffic corridors and commercial activity while not necessarily experiencing more episodic coarse bursts than nearby residential areas. At the same time, the broad within-group spreads visible in

Table 6: Residential–commercial differences in S_{NLR} (median difference, 95% bootstrap CI) within each season and location setting. Positive values indicate higher S_{NLR} in residential sites.

Location setting	**Season**	n_{Res}	n_{Com}	**Median difference (Res–Com) [95% CI]**
Suburban	DJF	159	44	-0.097 [-0.198, 0.032]
Suburban	MAM	175	53	-0.036 [-0.147, 0.066]
Suburban	JJA	175	57	-0.019 [-0.190, 0.101]
Suburban	SON	182	59	0.016 [-0.153, 0.085]
Urban and center city	DJF	100	93	0.101 [0.016, 0.220]
Urban and center city	MAM	105	106	0.006 [-0.070, 0.089]
Urban and center city	JJA	106	106	0.038 [-0.070, 0.165]
Urban and center city	SON	107	110	0.040 [-0.026, 0.076]

Fig. 5 caution against over-interpreting this reversal as a universal suburban mechanism; it may reflect heterogeneity in site placement and regional meteorology.

The mixture–exposure space view (Fig. 6) helps explain the overall pattern of weak land-use separation outside DJF. Residential and Commercial points strongly overlap in the (f_{med}, $\mathrm{PM}_{2.5,\mathrm{med}}$) plane, indicating that many station–season units share comparable fine/coarse regimes regardless of land-use label. Coarse-tail burstiness spans a wide range across both land uses, consistent with shared regional or meteorological drivers (e.g., resuspension, dust events, or sea-salt intrusions where relevant) that can affect multiple land-use contexts simultaneously.

Inspection of the distributional tails suggests that coarse-tail burstiness is an important differentiator at the extremes of S_{NLR}. High-S_{NLR} units tend to combine elevated $\mathrm{PM}_{2.5,\mathrm{med}}$ and/or f_{med} with lower B_c, whereas very large B_c can suppress S_{NLR} even when $\mathrm{PM}_{2.5,\mathrm{med}}$ or f_{med} are not especially low. This supports the practical value of including a coarse-tail penalty in a regime-oriented screening metric.

Finally, these results clarify both the strengths and the interpretative limits of S_{NLR} as a summary metric. Because the index combines typical exposure ($\mathrm{PM}_{2.5,\mathrm{med}}$), mixture structure ($f_{\mathrm{med}}$), and coarse-tail burstiness (B_c) in a single quantity, it provides a compact and interpretable way to compare station-scale mixture regimes across seasons and settings. At the same time, the substantial overlap between land-use categories indicates that S_{NLR} should not be interpreted as a strict classifier of Residential vs Commercial conditions under the present design.

The S_{NLR} is interpreted here as a screening and diagnostic index for station-scale fine–coarse mixture regimes derived from routine monitoring data. Importantly, the present study does not evaluate direct health outcomes, epidemiological associations, or regulatory exceedances (e.g., attainment/non-attainment decisions). Accordingly, any public-health relevance discussed in relation to seasonal or site-type contrasts remains inferential and should be considered hypothesis-generating pending formal epidemiological linkage and exposure–response analyses.

Benchmarking against simpler metrics indicates that S_{NLR} should not be interpreted as a universally superior discriminator in every stratum. Its practical value lies instead in providing a compact, regime-oriented summary that integrates partially distinct information from $\mathrm{PM}_{2.5,\mathrm{med}}$, fine fraction, and coarse-tail behavior while preserving the key contrasts emphasized in the present analysis.

Two design features are particularly important when interpreting these results. First, the land-use classes are broad and do not encode site adjacency to dominant sources (e.g., near-road, port/rail, or construction corridors), so residual misclassification is expected and may attenuate true differences. Second, aggregation to station–year–season improves robustness and reduces pseudo-replication, but necessarily averages over short-lived episodes; therefore, contrasts that are strong at daily scales (including dust or wildfire events) may be attenuated in the seasonal summaries used to compute S_{NLR}. From an applied standpoint, these results support using S_{NLR} as a compact indicator for screening persistent fine-dominant versus coarse-event-influenced regimes across monitoring networks, while motivating follow-on analyses that incorporate richer contextual covariates (meteorology, traffic intensity, near-road metrics, and regional stratification) to improve attribution and policy relevance.

An additional limitation is the absence of external source-regime validation in the present design. Because this study uses routine $\mathrm{PM}_{2.5}/\mathrm{PM}_{10}$ observations and broad station metadata strata without independent source-attribution labels at the station–season level, S_{NLR} should not be interpreted here as a validated source-classification metric. A priority for future work is to evaluate whether the index differentiates independently characterized regimes (e.g., dust-influenced vs traffic-dominated sites, or event-tagged periods) using external source or event annotations.

We therefore position the main novelty of the present work in the robustness-oriented station–season–year framework and its interpretable nonlinear integration of fine loading, fine fraction, and coarse-tail behavior, rather than in claiming that composite PM indices are new in general or that the chosen functional form is uniquely optimal.

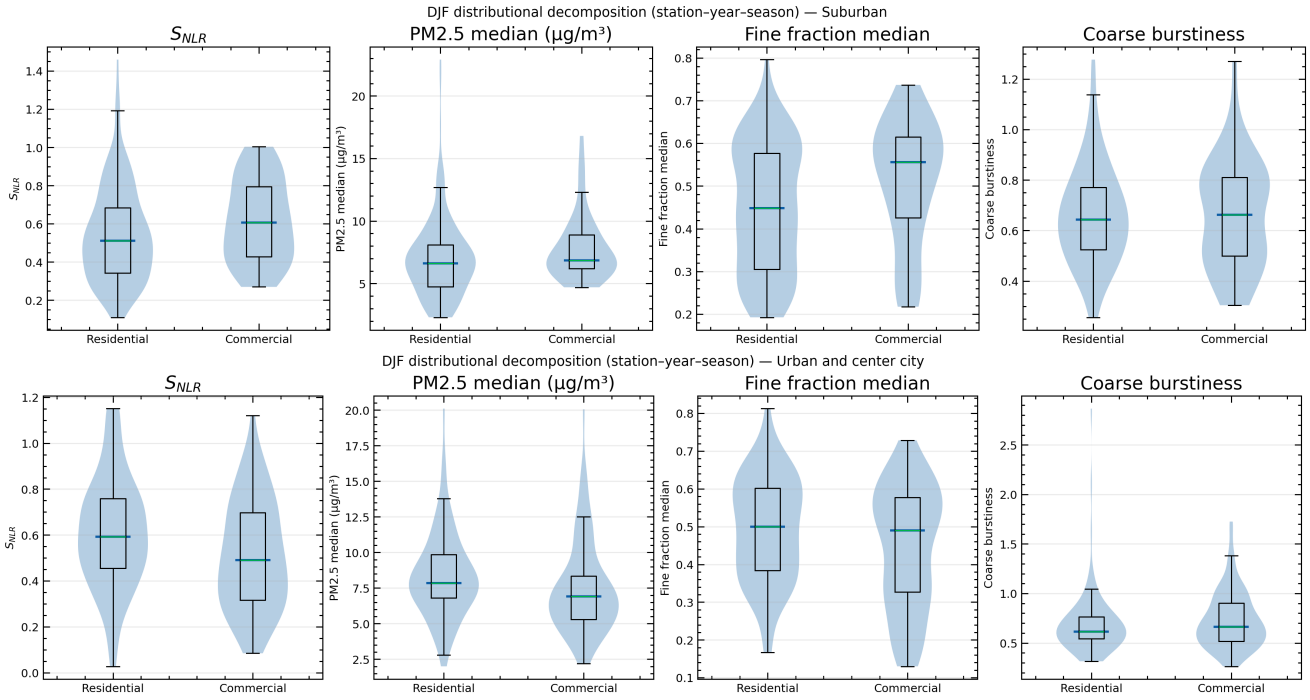

Figure 5: DJF distributional decomposition of S_{NLR} into mixture components. Panels summarize S_{NLR}, $\mathrm{PM}_{2.5,\mathrm{med}}$, fine-fraction median ($f_{\mathrm{med}} = \mathrm{median}(\mathrm{PM}_{2.5}/\mathrm{PM}_{10})$), and coarse-tail burstiness. Urban DJF shows the clearest Residential > Commercial separation in S_{NLR}, consistent with higher typical $\mathrm{PM}_{2.5}$ and fine fraction and modestly reduced coarse-tail burstiness.

4 Conclusions

This study introduced and applied a nonlinear robust index, S_{NLR}, to characterize fine–coarse mixture regimes using EPA AQS daily $\mathrm{PM}_{2.5}$ and PM_{10} data aggregated at the station–year–season level (2022–2024). By construction, S_{NLR} increases with higher typical fine fraction and higher typical $\mathrm{PM}_{2.5}$ exposure, while being penalized exponentially by coarse-tail burstiness. This decomposition provides an interpretable bridge between mixture composition and exposure intensity, allowing seasonal and land-use contrasts to be assessed with robust summaries and bootstrap uncertainty.

Across both location settings, the dominant empirical signal is seasonality: S_{NLR} is consistently lowest in MAM and highest in JJA, indicating systematic annual-cycle shifts in the balance between sustained fine-mode conditions and event-driven coarse variability. These seasonal patterns are substantially larger than typical Residential–Commercial differences, suggesting that meteorology and regional aerosol regimes are the primary controls of the station-level mixture signature at seasonal time scales. The mixture–exposure space analyses further show strong overlap between Residential and Commercial units, reinforcing that land-use labels alone do not uniquely determine mixture regime.

Land-use contrasts are generally modest and often indistinguishable from zero once uncertainty is considered, but one setting stands out: in Urban and center city during DJF, Residential sites exhibit higher S_{NLR} than Commercial sites, with a positive bootstrap confidence interval for the median difference. The DJF decomposition indicates that this separation is consistent with higher typical $\mathrm{PM}_{2.5}$ and fine fraction together with modestly reduced coarse-tail burstiness, implying more persistent fine-dominated conditions in residential urban wintertime environments. In suburban DJF the contrast trends in the opposite direction, but with overlapping uncertainty, highlighting substantial heterogeneity and the need for careful geographic and source-context stratification.

From an applied perspective, these results support using S_{NLR} primarily as a screening and diagnostic tool to identify station–season regimes characterized by persistent fine dominance versus regimes disrupted by episodic coarse events. For air-quality management, the findings emphasize that interventions targeting wintertime fine-particle persistence may be especially relevant in urban residential contexts, while strategies addressing coarse-tail burstiness (e.g., resuspension control, construction and road-dust mitigation, wind-sensitive operations) are important across land uses. Future work should (i) integrate meteorological covariates and regional clustering to separate synoptic

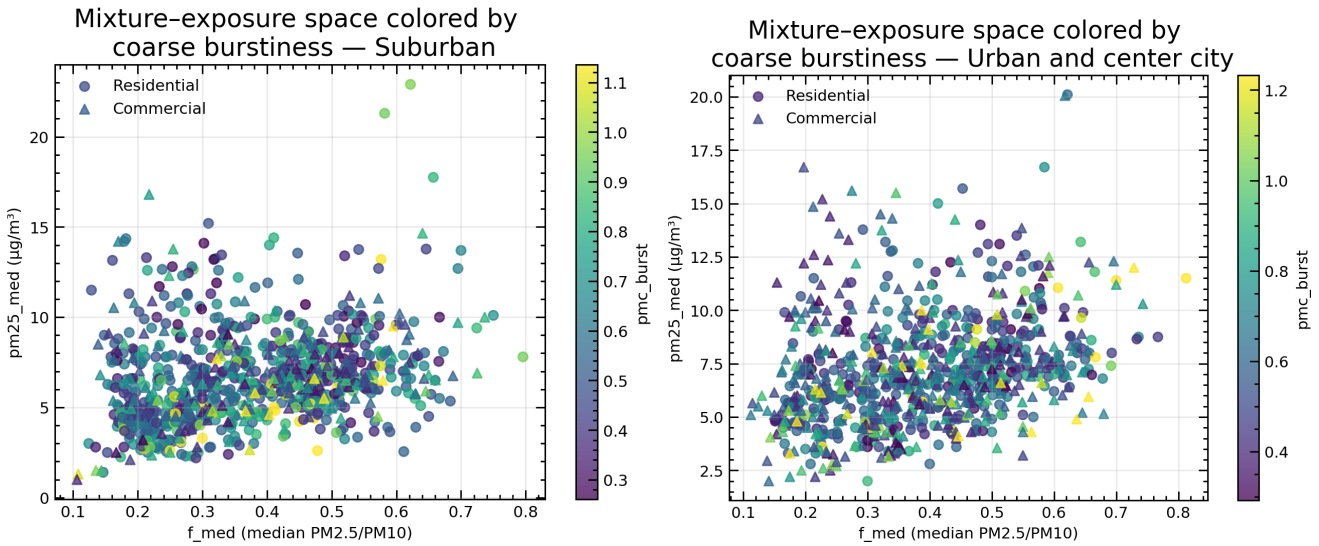

Figure 6: Mixture–exposure space (f_{med} vs $\mathrm{PM}_{2.5\mathrm{med}}$) colored by coarse-tail burstiness. Strong Residential/Commercial overlap indicates that land-use categories alone do not uniquely define mixture regime; episodic coarse behavior occurs across both classes and can limit systematic separation in S_{NLR}.

drivers from local effects, (ii) refine site characterization beyond coarse land-use classes (near-road metrics, distance-to-industrial/rail/port sources, population density), (iii) examine sensitivity to aggregation scale (monthly vs seasonal, event-based segmentation), and (iv) link S_{NLR} regimes to health-relevant outcomes or regulatory exceedances to quantify the public-health implications of fine-dominance persistence versus coarse-burst disruption.

Because no epidemiological linkage or regulatory exceedance analysis is performed here, the potential public-health and policy implications of S_{NLR} patterns should be interpreted as inferential and require dedicated follow-up studies.

Data and code availability

All raw data used in this study are fully open and publicly accessible through the U.S. EPA AirData/AQS portal. Specifically, we used the pre-generated daily summary archives for 2022–2024, including $\mathrm{PM}_{2.5}$ FRM/FEM mass (parameter code 88101; `daily_88101_YYYY.zip`), $\mathrm{PM}_{2.5}$ non-FRM/FEM mass (88502; `daily_88502_YYYY.zip`), PM_{10} mass (81102; `daily_81102_YYYY.zip`), and coarse PM (86101; `daily_86101_YYYY.zip`), downloadable from the EPA AirData files page (`https://aqs.epa.gov/aqsweb/airdata/download_files.html`). All tables and figures reported in this manuscript are reproducible from these open EPA archives using the processing steps described in the Methods.

Acknowledgments

We gratefully acknowledge the U.S. Environmental Protection Agency (EPA) for maintaining and openly publishing the AirData/AQS archives. The clarity of documentation, consistent data formatting, and long-term stewardship of these datasets make large-scale, reproducible analyses like this one possible. Any opinions, findings, and conclusions or recommendations expressed in this work are those of the authors and do not necessarily reflect the views of the EPA.

Conflict of Interest Statement

The authors declare that they have no conflict of interest.

CRediT author statement

D.S.-P.: Conceptualization, Methodology, Software, Validation, Formal analysis, Investigation, Resources, Data Curation, Writing - Original Draft, Writing - Review & Editing, Visualization, Supervision, Project administration, Funding acquisition. **I. S. A.-G.:** Methodology, Software, Formal analysis, Investigation, Data Curation, Writing - Original Draft. **J. F. G.-O.:** Methodology, Software, Formal analysis, Investigation, Data Curation, Writing - Original Draft. **E. A. N.-P.:** Software.

References

[1] U.S. Environmental Protection Agency. National ambient air quality standards (naaqs) for particulate matter (pm). https://www.epa.gov/pm-pollution/national-ambient-air-quality-standards-naaqs-pm, 2024. Accessed 2026-01-03.

[2] U.S. Environmental Protection Agency. Reconsideration of the national ambient air quality standards for particulate matter. https://www.federalregister.gov/documents/2024/03/06/2024-02637/reconsideration-of-the-national-ambient-air-quality-standards-for-particulate-matter, 2024. Accessed 2026-01-03.

[3] Yiqun Ma, Emma Zang, Yang Liu, Jing Wei, Yuan Lu, Harlan M Krumholz, Michelle L Bell, and Kai Chen. Long-term exposure to wildland fire smoke pm2. 5 and mortality in the contiguous united states. *Proceedings of the National Academy of Sciences*, 121(40):e2403960121, 2024. doi: https://doi.org/10.1073/pnas.2403960121.

[4] Wenhua Yu, Rongbin Xu, Tingting Ye, Michael J Abramson, Lidia Morawska, Bin Jalaludin, Fay H Johnston, Sarah B Henderson, Luke D Knibbs, Geoffrey G Morgan, et al. Estimates of global mortality burden associated with short-term exposure to fine particulate matter (pm2 · 5). *The Lancet Planetary Health*, 8(3):e146–e155, 2024. doi: https://doi.org/10.1016/S2542-5196(24)00003-2.

[5] Hongbin Yu, Qian Tan, Lillian Zhou, Yaping Zhou, Huisheng Bian, Mian Chin, Claire L. Ryder, Robert C. Levy, Yaswant Pradhan, Yingxi Shi, Qianqian Song, Zhibo Zhang, Peter R. Colarco, Dongchul Kim, Lorraine A. Remer, Tianle Yuan, Olga Mayol-Bracero, and Brent N. Holben. Observation and modeling of the historic "godzilla" african dust intrusion into the caribbean basin and the southern us in june 2020. *Atmospheric Chemistry and Physics*, 21:12359–12383, 8 2021. ISSN 16807324. doi: 10.5194/ACP-21-12359-2021.

[6] Souzana Achilleos, Petros Mouzourides, Nikos Kalivitis, Itzhak Katra, Itai Kloog, Panayiotis Kouis, Nicos Middleton, Nikos Mihalopoulos, Marina Neophytou, Andrie Panayiotou, Stefania Papatheodorou, Chrysanthos Savvides, Filippos Tymvios, Emily Vasiliadou, Panayiotis Yiallouros, and Petros Koutrakis. Spatio-temporal variability of desert dust storms in eastern mediterranean (crete, cyprus, israel) between 2006 and 2017 using a uniform methodology. *Science of the Total Environment*, 714, 4 2020. ISSN 18791026. doi: 10.1016/J.SCITOTENV.2020.136693.

[7] Shaniko Allajbeu, Flora Qarri, Elda Marku, Lirim Bekteshi, Vjollca Ibro, Marina V. Frontasyeva, Trajce Stafilov, and Pranvera Lazo. Contamination scale of atmospheric deposition for assessing air quality in albania evaluated from most toxic heavy metal and moss biomonitoring. *Air Quality, Atmosphere and Health*, 10:587–599, 6 2017. ISSN 18739326. doi: 10.1007/S11869-016-0453-9.

[8] Maria P. Velásquez-García, K. Santiago Hernández, James A. Vergara-Correa, Richard J. Pope, Miriam Gómez-Marín, and Angela M. Rendón. Long-range transport of air pollutants increases the concentration of hazardous components of pm2.5 in northern south america. *Atmospheric Chemistry and Physics*, 24:11497–11520, 10 2024. ISSN 16807324. doi: 10.5194/ACP-24-11497-2024.

[9] Vikas Rawat, Narendra Singh, Jaydeep Singh, Akanksha Rajput, Surendra K. Dhaka, Yutaka Matsumi, Tomoki Nakayama, and Sachiko Hayashida. Assessing the high-resolution pm2.5 measurements over a central himalayan site: impact of mountain meteorology and episodic events. *Air Quality, Atmosphere and Health*, 17:51–70, 1 2024. ISSN 18739326. doi: 10.1007/S11869-023-01429-7/METRICS. URL https://link.springer.com/article/10.1007/s11869-023-01429-7.

[10] Colin D. Butler and Ivan C. Hanigan. Air pollution, fires, climate change and health. *Climate Change and Global Health: Primary, Secondary and Tertiary Effects*, pages 242–259, 8 2024. doi: 10.1079/9781800620025.0020.

[11] Ava Orr, Claire E Adam, Jon Graham, Zachary A Holden, Lu Hu, Zeina Jaffar, Cindy Leary, Christopher T Migliaccio, Katrina Mullan, Curtis Noonan, et al. A state of the science review of wildfire-specific fine particulate matter data sources, methods, and models. *Environmental Health Perspectives*, 133(6):066001, 2025. doi: https://doi.org/10.1289/EHP15672.

[12] Ye Tian and Xiaobai Yao. Urban form, traffic volume, and air quality: A spatiotemporal stratified approach. *Environment and Planning B: Urban Analytics and City Science*, 49(1):92–113, 2022. doi: https://doi.org/10.1177/2399808321995822.

[13] Nazanin Rezaei and Adam Millard-Ball. Urban form and its impacts on air pollution and access to green space: A global analysis of 462 cities. *PloS one*, 18(1):e0278265, 2023. doi: https://doi.org/10.1371/journal.pone.0278265.

[14] Yiwen Wang, Xiaoyan Dai, Deming Gong, Liguo Zhou, Hao Zhang, and Weichun Ma. Correlations between urban morphological indicators and pm2. 5 pollution at street-level: implications on urban spatial optimization. *Atmosphere*, 15(3):341, 2024. doi: https://doi.org/10.3390/atmos15030341.

[15] Miguel Tarazona Alvarado, JL Salamanca-Coy, K Forero-Gutièrrez, LA Núñez, J Pisco-Guabave, Fr Escobar-Diaz, and David Sierra-Porta. Assessing and monitoring air quality in cities and urban areas with a portable, modular and low-cost sensor station: calibration challenges. *International Journal of Remote Sensing*, 45(17): 5713–5736, 2024. doi: https://doi.org/10.1080/01431161.2024.2373338.

[16] David Sierra-Porta, Yady Tatiana Solano-Correa, Miguel Tarazona-Alvarado, and Luis Alberto Nuñez de Villavicencio. Linking pm10 and pm2. 5 pollution concentration through tree coverage in urban areas. *CLEAN–Soil, Air, Water*, 51(5):2200222, 2023. doi: https://doi.org/10.1002/clen.202200222.

[17] Mohammad Kakooei and Yasser Baleghi. Spatial-temporal analysis of urban environmental variables using building height features. *Urban Climate*, 52:101736, 2023. doi: https://doi.org/10.1016/j.uclim.2023.101736.

[18] Daniel J. Kilpatrick, Peiyin Hung, Elizabeth Crouch, Stella Self, Jeremy Cothran, Dwayne E. Porter, and Jan M. Eberth. Geographic variations in urban-rural particulate matter (pm2.5) concentrations in the united states, 2010–2019. *GeoHealth*, 8:e2023GH000920, 9 2024. ISSN 2471-1403. doi: 10.1029/2023GH000920. URL `https://onlinelibrary.wiley.com/doi/full/10.1029/2023GH000920https://onlinelibrary.wiley.com/doi/abs/10.1029/2023GH000920https://agupubs.onlinelibrary.wiley.com/doi/10.1029/2023GH000920`.

[19] Alyssa M. Burns, Gabriel Chandler, Kira J. Dunham, and Annmarie G. Carlton. Data gap: Air quality networks miss air pollution from concentrated animal feeding operations. *Environmental Science and Technology*, 57:20718–20725, 12 2023. ISSN 15205851. doi: 10.1021/ACS.EST.3C06947/SUPPL_FILE/ES3C06947_SI_005.AVI. URL `https://pubs.acs.org/doi/full/10.1021/acs.est.3c06947`.

[20] JL Hand, AJ Prenni, SM Raffuse, NP Hyslop, WC Malm, and BA Schichtel. Spatial and seasonal variability of remote and urban speciated fine particulate matter in the united states. *Journal of Geophysical Research: Atmospheres*, 129(23):e2024JD042579, 2024. doi: https://doi.org/10.1029/2024JD042579.

[21] Nicholas Clements, Michael P. Hannigan, Shelly L. Miller, Jennifer L. Peel, and Jana B. Milford. Comparisons of urban and rural pm10-2.5 and pm2.5 mass concentrations and semi-volatile fractions in northeastern colorado. *Atmospheric Chemistry and Physics*, 16:7469–7484, 6 2016. ISSN 16807324. doi: 10.5194/ACP-16-7469-2016.

[22] Michelle L. Bell, Francesca Dominici, Keita Ebisu, Scott L. Zeger, and Jonathan M. Samet. Spatial and temporal variation in pm2.5 chemical composition in the united states for health effects studies. *Environmental Health Perspectives*, 115:989–995, 7 2007. ISSN 00916765. doi: 10.1289/EHP.9621/SUPPL_FILE/EHP.9621.S001.ACCO.PDF. URL `https://ehp.niehs.nih.gov/doi/10.1289/ehp.9621`.

[23] Richard A Kronmal. Spurious correlation and the fallacy of the ratio standard revisited. *Journal of the Royal Statistical Society Series A: Statistics in Society*, 156(3):379–392, 1993. doi: https://doi.org/10.2307/2983064.

[24] William C Malm, Bret A Schichtel, and Marc L Pitchford. Uncertainties in pm2. 5 gravimetric and speciation measurements and what we can learn from them. *Journal of the Air & Waste Management Association*, 61(11): 1131–1149, 2011. doi: https://doi.org/10.1080/10473289.2011.603998.

[25] Ningbo Jiang, Rinat Akter, Glenn Ross, Stephen White, John Kirkwood, Gunaratnam Gunashanhar, Scott Thompson, Matthew Riley, and Merched Azzi. On thresholds for controlling negative particle (pm2. 5) readings in air quality reporting. *Environmental Monitoring and Assessment*, 195(10):1187, 2023. doi: https://doi.org/10.1007/s10661-023-11750-4.

[26] Wanyun Xu, Ye Kuang, Linlin Liang, Yao He, Hongbing Cheng, Yuxuan Bian, Jiangchuan Tao, Gen Zhang, Pusheng Zhao, Nan Ma, Huarong Zhao, Guangsheng Zhou, Hang Su, Yafang Cheng, Xiaobin Xu, Min Shao, and Yele Sun. Dust-dominated coarse particles as a medium for rapid secondary organic and inorganic aerosol formation in highly polluted air. *Environmental Science and Technology*, 54:15710–15721, 12 2020. ISSN 15205851. doi: 10.1021/ACS.EST.0C07243/SUPPL_FILE/ES0C07243_SI_001.PDF. URL https://pubs.acs.org/doi/abs/10.1021/acs.est.0c07243.

[27] U.S. Environmental Protection Agency. Download daily data. https://www.epa.gov/outdoor-air-quality-data/download-daily-data, 2025. Accessed 2026-01-03.

[28] U.S. Environmental Protection Agency. What is the difference between parameter codes 88101 and 88502 for $pm_{2.5}$ monitors?, December 2025. URL https://www.epa.gov/outdoor-air-quality-data/what-difference-between-parameter-codes-88101-and-88502-pm25-monitors. Accessed 2026-01-03.

[29] U.S. Environmental Protection Agency. Aqs code list, 2025. URL https://www.epa.gov/aqs/aqs-code-list. Accessed 2026-01-03.

[30] Electronic Code of Federal Regulations. 40 cfr part 58, appendix a: Quality assurance requirements for state and local air monitoring stations, 2026. URL https://www.ecfr.gov/current/title-40/chapter-I/subchapter-C/part-58/appendix-Appendix%20A%20to%20Part%2058. Accessed 2026-01-03.

[31] Stuart H. Hurlbert. Pseudoreplication and the design of ecological field experiments. *Ecological Monographs*, 54 (2):187–211, 1984. doi: https://doi.org/10.2307/1942661.

[32] Hannah McKinnon Reish, Lindsey Dewey, and Lucas J. Kirschman. A host of issues: pseudoreplication in host-microbiota studies. *Applied and Environmental Microbiology*, 90(8):e01033–24, 2024. doi: https://doi.org/10.1128/aem.01033-24. Epub 2024-07-31.

[33] BEYHAN Pekey, ZB Bozkurt, HAKAN Pekey, GÜRAY Doğan, Abdullah Zararsız, N Efe, and G Tuncel. Indoor/outdoor concentrations and elemental composition of pm10/pm2. 5 in urban/industrial areas of kocaeli city, turkey. *Indoor air*, 20(2):112–125, 2010. doi: https://doi.org/10.1111/j.1600-0668.2009.00628.x.

[34] Xavier Jurado, Nicolas Reiminger, Loïc Maurer, José Vazquez, and Cédric Wemmert. On the correlations between particulate matter: Comparison between annual/monthly concentrations and pm10/pm2. 5. *Atmosphere*, 14(2):385, 2023. doi: https://doi.org/10.3390/atmos14020385.

[35] U.S. Environmental Protection Agency. Quality assurance handbook for air pollution measurement systems, volume ii: Ambient air quality monitoring program. Technical Report EPA-454/B-17-001, U.S. Environmental Protection Agency, Office of Air Quality Planning and Standards, January 2017. URL https://www.epa.gov/sites/default/files/2020-10/documents/final_handbook_document_1_17.pdf.

[36] U.S. Environmental Protection Agency. Best practices for review and validation of ambient air monitoring data. Technical Report EPA-454/B-21-007, U.S. Environmental Protection Agency, Office of Air Quality Planning and Standards, August 2021. URL https://www.epa.gov/system/files/documents/2021-10/data-validation-guidance-document-final-august-2021.pdf.

[37] U.S. Environmental Protection Agency. Epa data validation templates (appendix d): Validation template, version 03 (march 2017), revision 1. Technical report, U.S. Environmental Protection Agency, March 2017. URL https://www.epa.gov/sites/default/files/2020-10/documents/app_d_validation_template_version_03_2017_for_amtic_rev_1.pdf. Often distributed via AMTIC as Appendix D validation template.

[38] Bradley Efron and Robert J. Tibshirani. *An Introduction to the Bootstrap*. Chapman & Hall/CRC, 1993. ISBN 978-0412042317.

[39] U.S. Environmental Protection Agency. Airdata: Download files (pre-generated daily summary archives), 2025. URL https://aqs.epa.gov/aqsweb/airdata/download_files.html. Accessed 2026-01-03.

[40] U.S. Environmental Protection Agency. Obtaining aqs data, 2025. URL https://www.epa.gov/aqs/obtaining-aqs-data. Accessed 2026-01-03.

[41] Nathan Hilker, Jonathan M Wang, Cheol-Heon Jeong, Robert M Healy, Uwayemi Sofowote, Jerzy Debosz, Yushan Su, Michael Noble, Anthony Munoz, Geoff Doerksen, et al. Traffic-related air pollution near roadways: discerning local impacts from background. *Atmospheric Measurement Techniques*, 12(10):5247–5261, 2019. doi: https://doi.org/10.5194/amt-12-5247-2019.

[42] Peng Wei, Peter Brimblecombe, Fenhuan Yang, Abhishek Anand, Yang Xing, Li Sun, Yuxi Sun, Mengyuan Chu, and Zhi Ning. Determination of local traffic emission and non-local background source contribution to on-road air pollution using fixed-route mobile air sensor network. *Environmental Pollution*, 290:118055, 2021. doi: https://doi.org/10.1016/j.envpol.2021.118055.

[43] Guillaume Rousselet, Cyril R Pernet, and Rand R Wilcox. An introduction to the bootstrap: a versatile method to make inferences by using data-driven simulations. *Meta-Psychology*, 7, 2023. doi: https://doi.org/10.15626/MP.2019.2058.

[44] Jacob W Maddison, Marta Abalos, David Barriopedro, Ricardo García-Herrera, Jose M Garrido-Perez, and Carlos Ordóñez. Linking air stagnation in europe with the synoptic-to large-scale atmospheric circulation. *Weather and Climate Dynamics*, 2(3):675–694, 2021. doi: https://doi.org/10.5194/wcd-2-675-2021.

[45] Jose M Garrido-Perez, Carlos Ordóñez, Ricardo García-Herrera, and David Barriopedro. Air stagnation in europe: spatiotemporal variability and impact on air quality. *Science of The Total Environment*, 645:1238–1252, 2018. doi: https://doi.org/10.1016/j.scitotenv.2018.07.238.

[46] Gregori de Arruda Moreira, Marcia Talita Amorim Marques, Fabio Juliano da Silva Lopes, Maria de Fátima Andrade, and Eduardo Landulfo. Analyzing the influence of the planetary boundary layer height, ventilation coefficient, thermal inversions, and aerosol optical depth on the concentration of pm2. 5 in the city of são paulo: A long-term study. *Atmospheric Pollution Research*, 15(8):102179, 2024. doi: https://doi.org/10.1016/j.apr.2024.102179.

[47] Hengheng Zhang, Wei Huang, Xiaoli Shen, Ramakrishna Ramisetty, Junwei Song, Olga Kiseleva, Christopher Claus Holst, Basit Khan, Thomas Leisner, and Harald Saathoff. Aerosol composition, air quality, and boundary layer dynamics in the urban background of stuttgart in winter. *Atmospheric Chemistry and Physics*, 24(18):10617–10637, 2024. doi: https://doi.org/10.5194/acp-24-10617-2024.

[48] Jialin Yao, Xingcan Jia, and Zhiheng Liao. Exploring the impact of nocturnal boundary layer stability on wintertime air pollution in a highly polluted basin city using unsupervised learning classification. *Atmospheric Pollution Research*, 15(10):102253, 2024. doi: https://doi.org/10.1016/j.apr.2024.102253.